Sixth International Symposium on Turbulence and Shear Flow Phenomena
Seoul, Korea, 22-24 June 2009

MULTI-SCALE COHERENT STRUCTURES OF SPATIALLY ADVANCING TURBULENT FLOWS IN CURVED CHANNEL

Koji Matsubara, Akihiko Matsui, Takahiro Miura, Koji Kawai, Mutsuo Kobayashi
Department of Mechanical and Production Engineering,
Niigata University
Ikarashi 2-nocho 8050, Nishi-ku, Niigata-shi 950-2181, Japan
matsu@eng.niigata-.ac.jp

Hitoshi Suto
Fluid Dynamic Sector, Civil Engineering Research Laboratory,
Central Research Institute of Electric Power Industry
1646 Abiko, Abiko-shi, Chiba-ken 270-1194, Japan
suto@criepi.denken.or.jp

ABSTRACT

Direct numerical simulation was performed for the spatially advancing turbulent flow in a two-dimensional curved channel. The inlet flow of the curved channel was the fully developed turbulence which was additively simulated by the straight channel driver. The radius ratio of the curved part, α, was set 0.92, and the frictional Reynolds number, $Re_{\tau 0}$, was assigned 150. Computational volume was changed in three kinds of its spanwise extent. However, discussion was mainly given to the prediction by the largest extent (7.2 times the channel half width) where 512 x 61 x 128 grid points were allocated. Computationally solved mean velocity and other statistics showed trends generally consistent with the experiment by Kobayashi et al. (1991), and the numerical validity was thus confirmed. Time-mean velocity vectors illustrated that the ejection from the outer wall grows into the organized flow of the large-scale streamwise vortices. The power spectrum analysis implied that the fine-scale structures such as the low-speed streaks and the microscopic ejection near the outer wall of the straight channel created the initial seeds of the organized wave which grew the large scale vortices extending almost over the channel width.

INTRODUCTION

Fundamental physics of turbulent flows over a curved surface are needed in designing and developing the thermo-fluid machineries such as turbine blades and heat exchangers. Such information can be applied for flow control on airplane blades and automobiles. Therefore, efforts have been made for revealing flow structures near the curvature of its laminar cases (for example, Ligrani and Niver, 1988) and of its turbulent cases. Kobayashi et al. (1991) measured turbulence statistics by hot-wire anemometry, and they pointed out that, in the developed flow of the curved channel, turbulence quantities are controlled by organized motion of large-scale vortex. Moser and Moin (1987) directly solved the Navier-Stokes equation, and they captured complete data of the low-Reynolds-number turbulence in the curved channel. However, they assumed streamwise periodicity of the curved flow, and there was left ambiguity on growing process of the large-scale vortices.

In this paper, spatially advancing type of DNS is performed for the two-dimensional curved channel. The geometry treated is the same as the experiment by Kobayashi et al. (1991). However, the Reynolds number is kept roughly one fourths of the experiment in order to resolve all the essential scale of turbulence. Various kinds of turbulence statistics including power spectrum is presented. Examination is given to the advancement of the large scale vortex and the transition of the near-wall coherent structures such as the low-speed streaks and the quasi-streamwise micro eddies.

NOMENCLATURE

E_w : power spectrum of wall-normal velocity [m^3/s^2]
k_z : wave number in spanwise direction [1/m]
L_x, L_y, L_z : computational domain size in x, y, z [m]
$Re_{\tau 0}$: frictional Reynolds number $U_\tau \delta / \nu$
r : wall-normal coordinate [m]
r_i, r_o : curvature radius of inner and outer wall [m]
r_m : mean curvature radius = ($r_i + r_o$) / 2 [m]
t : time [s]
U,V,W : velocity [m/s]
U_τ : frictional velocity [m/s]
$U_{\tau 0}$: frictional velocity in straight channel [m/s]
u , v ,w : velocity fluctuation in x, y, z [m/s]
x : streamwise coordinate = $r_m \phi$ [m]
y : wall-normal coordinate =r-r_i[m]
z : spanwise coordinate [m]
α : radius ratio = r_i / r_o
δ : channel half width [m]
λ_z : wave length in spanwise direction [m]
ν : kinematic viscosity [m^2/s]

σ : non-dimensional number = $2\alpha/(1-\alpha)$
ϕ : streamwise coordinate [°], [rad]
rms : fluctuation intensity
*: non-dimensionalization by δ and $U_{\tau 0}$
+ : non-dimensionalization by U_τ and ν
++ : non-dimensionalization by $U_{\tau 0}$ and ν

COMPUTATIONAL SCHEME

Figure 1 shows the two-dimensional curved channel and the computational domain. Consider the curved channel continuously connected to the inlet part of the straight channel. In order to simulate this situation by the minimum computational load, the straight and the curved channel are separately treated. The fully developed turbulence solved by the straight driver was given to the inlet boundary of the curved-channel simulator (Ohta and Kajishima, 2004; Hattori et al., 2007).

In the straight part, periodicity condition was used not only for the streamwise direction but also for the spanwise direction, while, in the curved part, similar condition only for the streamwise direction. The radius ratio, $\alpha(=r_i/r_o)$, was set 0.92 the same as Kobayashi et al. (1991), where r_i and r_o represent, respectively, the curvature radius of the inner and the outer wall. The Reynolds number based on the friction velocity and the channel half width, $Re_{\tau 0}$, was given 150. By the straight-channel DNS with this condition, the Reynolds number based on the mean velocity and the channel width was computed 4,530.

In Fig. 1, coordinates (x, y, z) correspond to the Cartesian system in the straight part, but to the cylindrical system (ϕ, r, z) in the curved part. The relation between two systems is written in the nomenclature. In the following, the velocity components for (x, y, z) are expressed by (U, V, W).

The governing equations used in the simulation were the continuity, Navier-Stokes equations;

$$\frac{\sigma+1}{y^*+\sigma}\frac{\partial U^{++}}{\partial x^*}+\frac{\partial V^{++}}{\partial y^*}+\frac{V^{++}}{y^*+\sigma}+\frac{\partial W^{++}}{\partial z^{**}}=0, \qquad (1)$$

$$\frac{\partial U^{++}}{\partial t^*}+\frac{\sigma+1}{y^*+\sigma}U^{++}\frac{\partial U^{++}}{\partial x^*}+V^{++}\frac{\partial U^{++}}{\partial y^*}+\frac{U^{++}V^{++}}{y^*+\sigma}+$$
$$W^{++}\frac{\partial U^{++}}{\partial z^*}=-\frac{\sigma+1}{\sigma+y^*}\frac{\partial P^{++}}{\partial x^{**}}+\frac{1}{Re_{\tau 0}}\left\{\left(\frac{\sigma+1}{y^*+\sigma}\right)^2\frac{\partial^2 U^{++}}{\partial x^{*2}}\right.$$
$$\frac{2(\sigma+1)}{(y^*+\sigma)^2}\frac{\partial V^{++}}{\partial x}+\frac{\partial^2 U^{++}}{\partial y^{*2}}+\frac{1}{y^*+\sigma}\frac{\partial U^{++}}{\partial y^{**}}-\frac{U^{++}}{(y^*+\sigma)^2}$$
$$\left.+\frac{\partial^2 U^{++}}{\partial z^{*2}}\right\}, \qquad (2)$$

$$\frac{\partial V^{++}}{\partial t^*}+\frac{\sigma+1}{y^*+\sigma}U^{++}\frac{\partial V^{++}}{\partial x^*}+V^{++}\frac{\partial V^{++}}{\partial y^*}-\frac{U^{++2}}{y^*+\sigma}+$$
$$W^{++}\frac{\partial V^{++}}{\partial z^*}=-\frac{\partial P^{++}}{\partial y^{**}}+\frac{1}{Re_{\tau 0}}\left\{\left(\frac{\sigma+1}{y^*+\sigma}\right)^2\frac{\partial^2 V^{++}}{\partial x^{*2}}-\right.$$
$$\frac{2(\sigma+1)}{(y^*+\sigma)^2}\frac{\partial U^{++}}{\partial x}+\frac{\partial^2 V^{++}}{\partial y^{*2}}+\frac{1}{y^*+\sigma}\frac{\partial V^{++}}{\partial y^{**}}-\frac{V^{++}}{(y^*+\sigma)^2}$$
$$\left.+\frac{\partial^2 V^{++}}{\partial z^{*2}}\right\}, \qquad (3)$$

$$\frac{\partial W^{++}}{\partial t^*}+\frac{\sigma+1}{y^*+\sigma}U^{++}\frac{\partial W^{++}}{\partial x^*}+V^{++}\frac{\partial W^{++}}{\partial y^*}+$$
$$W^{++}\frac{\partial W^{++}}{\partial z^*}=-\frac{\partial P^{++}}{\partial z^{**}}+\frac{1}{Re_{\tau 0}}\left\{\left(\frac{\sigma+1}{y^*+\sigma}\right)^2\frac{\partial^2 W^{++}}{\partial x^{*2}}+\right.$$
$$\left.+\frac{\partial^2 W^{++}}{\partial y^{*2}}+\frac{1}{y^*+\sigma}\frac{\partial W^{++}}{\partial y^{**}}+\frac{\partial^2 W^{++}}{\partial z^{*2}}\right\}. \qquad (4)$$

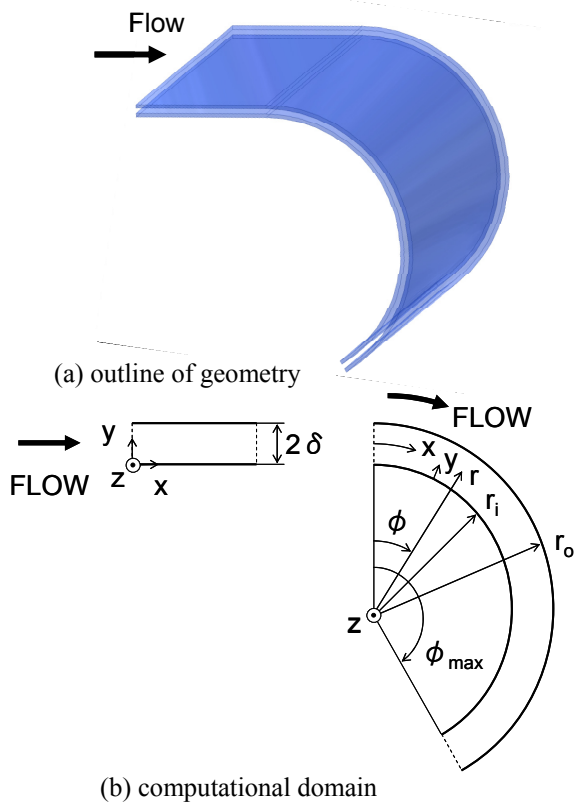

(a) outline of geometry

(b) computational domain

Fig. 1 Two-dimensional curved channel.

Table 1 Computational condition of straight channel.

case	$Re_{\tau 0}$	L_x/δ	L_y/δ	L_z/δ	resolution
1	150	3.92	2	1.80	32x61x32
2	150	3.92	2	3.60	32x61x64
3	150	3.92	2	7.20	32x61x128

Table 2 Computational condition of curved channel.

case	α	$\Phi_{\max}$	average time	resolution
1	0.92	150°	$40\delta/U_{\tau 0}$	512x61x32
2	0.92	150°	$100\delta/U_{\tau 0}$	512x61x64
3	0.92	150°	$38.8\delta/U_{\tau 0}$	512x61x128

In these equations, coordinates are non-dimensionalized by the channel half width, δ, and the velocity by the frictional velocity, $U_{\tau 0}$. In equations (1) to (4), non-dimensional value, $\sigma(=r_i/\delta=2\alpha/(1-\alpha))$, is used for simplicity in expression. Note that equations (1) to (4) are compatible with the Cartesian formulas when $\alpha \to 1.0$ ($\sigma \to \infty$).

In the simulation, the equations (1) to (4) were integrated by the fractional time step method (Kim and Moin, 1985), where the Crank-Nicolson method was adopted for the wall-normal second derivatives and the Adams-Bashforth method for other terms. The forth order central differencing was applied for all the spatial derivatives of the equations (Matsubara et al., 1998). To solve the Poisson equation for pressure in the driver, the Fast Fourier Transformation (FFT) was adopted for x and z direction with the 4th order compact difference in y direction. However, the pressure in the curved channel was solicited through the FFT in z direction and the 4th-order difference combined with SOR in x-y plane.

Table 1 and table 2 show computational condition. The spanwise length of the channel, L_z, was changed in three steps; 1.8, 3.6 and 7.2 times the channel half width, δ. However, turbulence statistics did not show essential change for three cases. In the following part, the numerical data are cited from the simulation by L_z/δ=7.2, where 512x61x128 grids are allocated in the main simulator. In the simulation of the straight driver, the turbulence statistics including the Reynolds stress budget agreed well with the spectral method (Kasagi et al., 1992), which supported the validity of the grids and the basic performance of the computational code.

RESULTS AND DISCUSSION

Mean Velocity

Figure 2 shows the radial distribution of the mean velocity at six angles in the curved channel plus that in the straight driver. This figure and the followings are ones presenting the numerical results of L_z/δ=7.2 (case 3) as earlier mentioned.

In Fig. 2, the key point of the mean behavior is the flow acceleration near the outer wall but with the deceleration near the inner wall. This is caused by that the flow is inclined nearer to the outer wall, more apart from the inner wall, with the flow advancement under the bending effect by the channel. Mean velocity distribution is almost flat in the channel center region of $\phi \geqq 75^\circ$. This suggests activity of the convective mixing through the organized flow later mentioned.

Figure 3 shows friction velocity in the curved channel. The friction velocity decreases on the inner wall, and it increases on the outer wall. There is mostly 40% difference between two walls for $\phi \geqq 60^\circ$. In this part, values on two

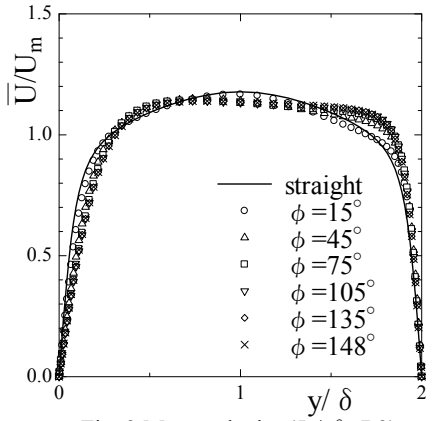

Fig. 2 Mean velocity (L_z/δ=7.2).

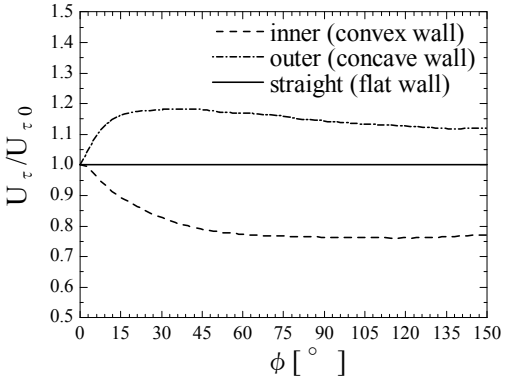

Fig. 3 Wall friction velocity (L_z/δ=7.2).

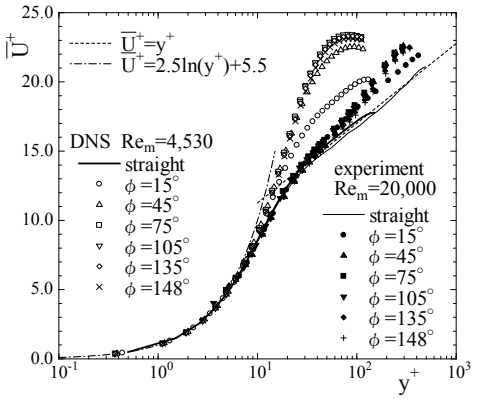

Fig. 4 Mean velocity for inner wall side (L_z/δ=7.2).

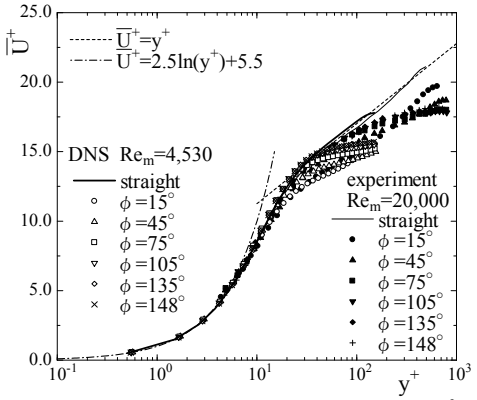

Fig. 5 Mean velocity for outer wall side (L_z/δ=7.2).

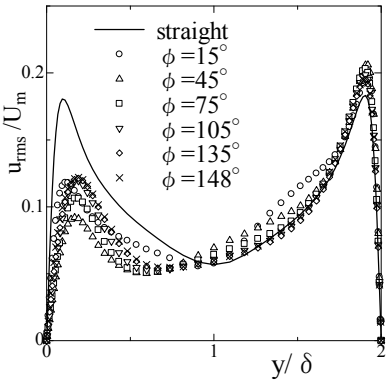

Fig. 6 Streamwise turbulent intensity (L_z/δ=7.2).

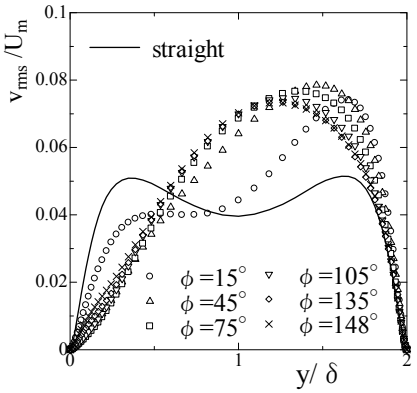

Fig. 7 Radial turbulent intensity (L_z/δ=7.2).

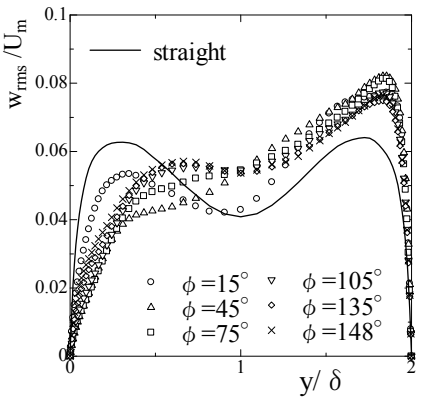

Fig. 8 Spanwise turbulent intensity (L_z/δ=7.2).

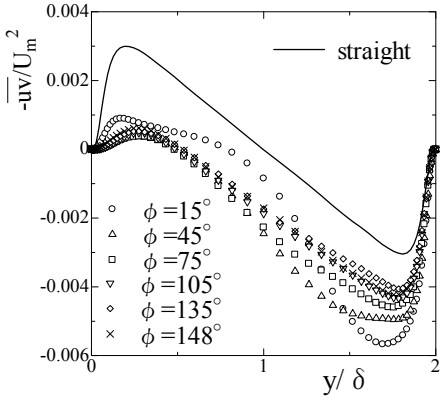

Fig. 9 Reynolds shear stress (L_z/δ=7.2).

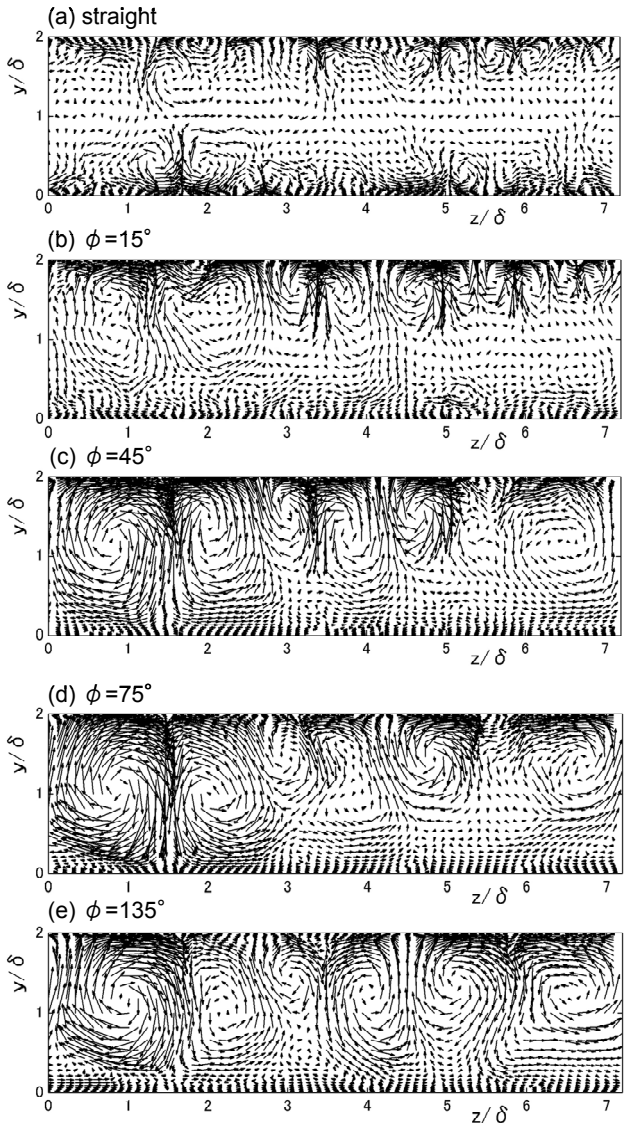

Fig. 10 Time mean velocity vectors in y-z plane (L_z/δ=7.2).

walls slightly get closer, but they keep constancy, if coarsely observed, denoting the flow establishment.

Mean velocity is normalized by the local friction velocity, and its inner-side value is plotted in Fig. 4 together with the experimental data by Kobayashi et al. (1991). Similar plot is made for its outer-side value in Fig. 5. In these figures, the numerical simulation and the experiment are generally consistent in spite of the Reynolds number difference. Both results show offset of logarithmic velocity from the universal law; the upward offset in the outer side of the channel and the downward offset in the inner side of it. Similar trends are observed in the laminarization of turbulent flow (Iida and Nagao, 1998) and the rotating flow (Kristoffersen and Andersson, 1993), and the combined effects from laminarization and rotation should work in the present case. Quantitative gap between DNS and the experiment occurred in the inner side of channel. This is

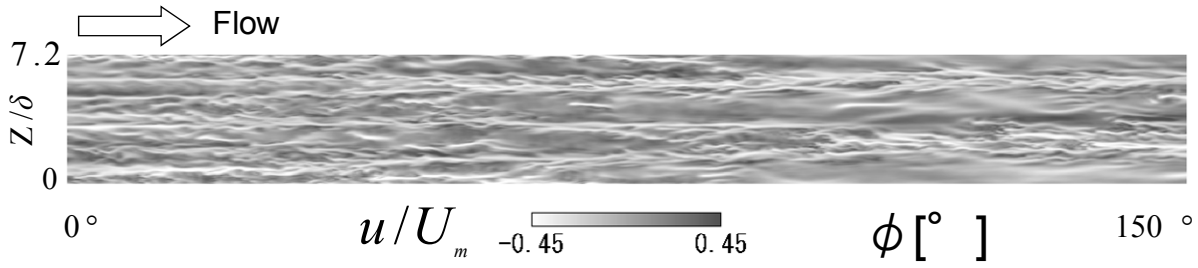

Fig. 11 Streamwise velocity fluctuation at y/δ=1.92 (L_z/δ=7.2) .

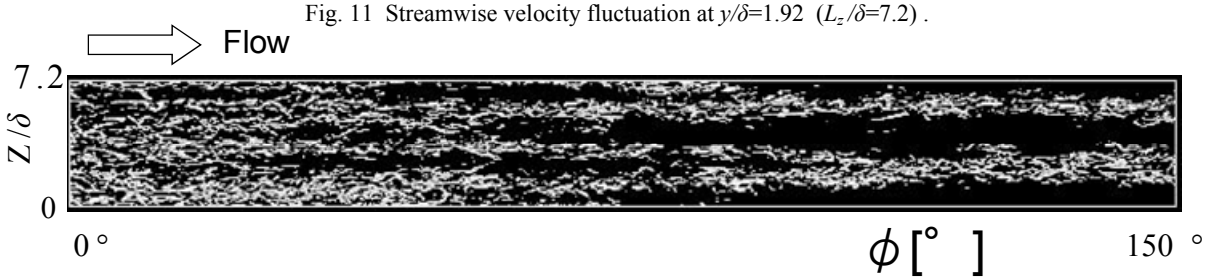

Fig. 12 Iso-surface of second invariance of velocity gradient tensor Π^{++} = 0.005 (L_z/δ=7.2) .

caused by the stronger laminarization which was resulted from the lower Reynolds number prescribed in the simulation than in the experiment.

Turbulent Intensity and the Reynolds shear stress

The turbulent intensity and the Reynolds shear stress are plotted in Figs 6-9. Just after the inflow to the curved channel, streamwise component of the turbulent intensity is enhanced near the outer wall, while it is reduced near the inner wall. In the inner wall-side, this component starts to resurge at ϕ =75° , showing almost no change for $\phi \geqq$ 135° . This resurgence of the streamwise component is due to the organized vortices later mentioned. This kind of the vortices should act as the conveyor of the fine-scale eddies which are created in the outer-wall side of the channel going to the inner-wall side of it.

Other components of the turbulent intensity and the Reynolds shear stress show trends similar to the streamwise component. However, v_{rms} and w_{rms} are affected by the secondary flow motion more strongly than the streamwise component, and their behaviors are more complex. The peak of v_{rms} in the outer-wall side moves to the channel center with the advancement of the curved flow, and the peak of w_{rms} in the inner-wall side once decreases but recovering with its spatial transport toward the channel center. These behaviors are resulted from the convective effect of organized vortices, which are initially small-scale eddies near the outer wall, growing and prevailing mostly all over the channel width. In spite of the Reynolds number difference, there is consistency between DNS and the previous experiment (Kobayashi et al., 1991) in major characteristics above mentioned.

Flow Structures

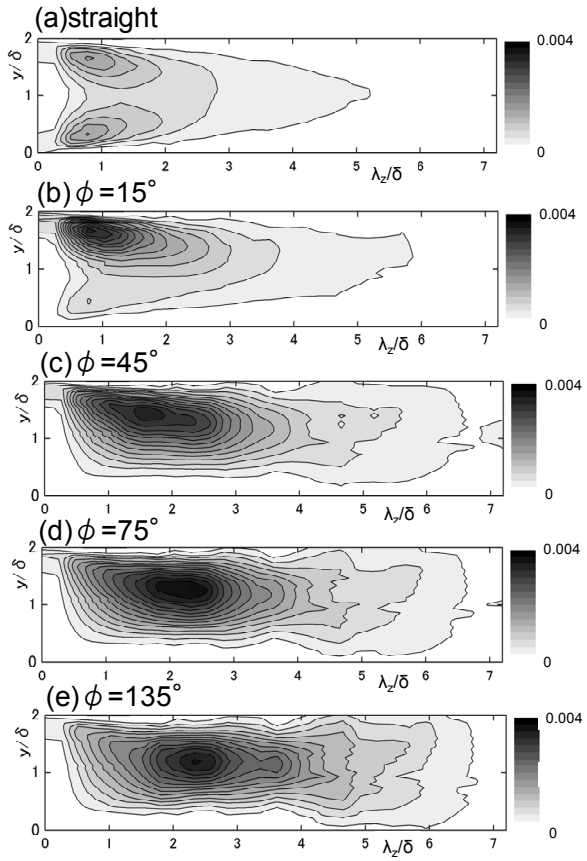

Fig. 13 Spanwise pre-multiplied power spectra of wall-normal velocity, $k_z E_{vvz}/U_m^2$, (L_z/δ=7.2).

Figure 10 shows the velocity vectors in five sets of y-z plane, where, for clear observation, irregularity was removed by the time filter corresponding to 10 times of the dissipation time scale. In the straight part, there are about eight realizations of ejection near the two walls each, and they accompany streamwise vortices. When the flow goes

into the curved channel, the velocity fluctuation near the inner wall decays, but enhances near the outer wall. Near the outer surface, ejecting motion grows in its size and strength as the channel angle, ϕ, proceeds. For $\phi \geqq 45°$ six realizations of large-scale vortices can be observed. This process implies that the micro-scale ejection and the accompanied eddies in the straight channel are seeds of the organized structures developing into large-scale eddies extending nearly the whole channel width.

In order to observe low-speed streaks, fluctuation of streamwise velocity is visualized by the contour map near the outer wall (y/δ=1.92) in Fig. 11. The fine-scale eddies are detected by the second invariant of the velocity gradient tensor, and its iso-surfaces are depicted in Fig. 12. As the flow advances downstream, the low-speed streaks merge their neighboring structures, going into thicker band, and small-scale eddies close to the streak lines are engulfed into converged band of the streaks. Comparison with Fig. 10 reveals that the large-scale ejection from the outer wall, which was previously mentioned, occurs just at the low-speed region, and the small-scale eddies are convened by the spanwise convection of the large-scale circulation. Therefore, the flow in the curved channel exhibits multi-scale structures of turbulence due to the superimposition of large-scale motions and micro-scale eddies.

Figure 13 shows the spanwise spectrum of pre-multiplied power for the wall-normal velocity. This component was selected because it clearly detects the large-scale motion as suggested in Fig. 10. In the straight part, a peak position at the spanwise wave length λ_z=0.8δ expresses space between low-speed streaks. As channel angle increases from ϕ=15° to ϕ=75°, the peak moves away from the outer wall with its wave length shift from 1.0 δ to 2.0 δ. At ϕ=135°, power spectrum takes peak at 2.2 δ, mostly corresponding to double the spanwise extent of large-scale eddies in Fig. 10. Continuous growth of power spectrum supports the previously extracted dynamics such that micro-scale ejections with micro-scale eddies enhance its size and strength, which develops into the organized wave of the large-scale eddies mostly over the channel width.

CONCLUSIONS

Direct numerical simulation was performed for the curved channel turbulent flow of the frictional Reynolds number equal to 150 at the channel inlet. Major findings are as follows.

(1) Numerically solved mean velocity and the turbulence statistics showed trends consistent with the experiment by Kobayashi et al. (1991) in spite of the Reynolds number difference. Major skeleton of the flow was thus common regardless of the Reynolds number.

(2) Instantaneous flow field included not only organized large-scale flow but also fine-scale irregularity. The time mean velocity field showed that micro-scale ejection from the outer wall and accompanied twin vortices became larger and stronger, as the flow advanced in the curved channel.

(3) Instantaneous flow field showed that the low-speed streaks and the fine-scale eddies near the outer wall were enrolled by the spanwise convection of the large-scale circulation and concentrated into the bands of converged streaks.

(4) The spanwise spectrum of pre-multiplied power indicated that the fluctuation corresponding to the streaky structures are initially enhanced in the curved channel and this scale of fluctuation developed stronger, having larger wave-length. This and conclusions (2) and (3) denoted that small-scale ejections accompanied by small-scale eddies were seeds of organized motion which developed into large-scale vortices extending mostly over the channel width.

REFERENCES

Hattori, H. and Houra, T. and Nagano, Y., 2007, "Direct Numerical Simulation of Stable and Unstable Turbulent Thermal Boundary Layers", *Heat and Fluid Flow*, Vol. 28, pp. 1262-1271.

Iida, O. and Nagano, Y., 1998, "The Relaminarization Mechanisms of Turbulent Channel Flow at Low Reynolds Number", *Flow, Turbulence and Combustion*, Vol. 60, pp. 193-213.

Kasagi, N., Tomita, Y. and Kuroda, 1992, "A., Direct Numerical Simulation of Passive Scalar Transport in a Turbulent Channel Flow", *ASME J. Heat Transfer*, Vol. 114, pp. 598-606.

Kim, J. and Moin, P., 1985, "Application of a Fractional Step Method to Incompressible Navier-Stokes Equations", *J. Comput. Phys*, Vol. 59, pp. 308-323.

Kobayashi, K., Maekawa, H., Takano, T. and Hayakawa, S., 1991, "An Experimental Study on a Turbulent Flow in a Two-Dimensional Curved Channel (Time-Mean Velocity and Multiple Velocity Correlations in the Entrance Section)", *Transactions of the Japan Society of Mechanical Engineers, Series B*, Vol. 57, No. 544, pp. 4064-4071.

Kristoffersen, R. and Andersson, H. I., 1993, "Direct Simulations of Low-Reynolds-Number Turbulent Flow in a Rotating Channel", *J. Fluid Mech.*, Vol. 256, pp. 163-197.

Ligrani, P. M. and Niver, R. D., 1988, "Flow Visualization of Dean Vortices in a Curved Channel with 40 to 1 Aspect Ratio", *Phys Fluids*, Vol. 31, No. 12, pp. 3605-3617.

Matsubara, K., Kobayashi, M. and Maekawa, H., 1998, "Direct Numerical Simulation of a Turbulent Channel Flow with a Linear Spanwise Mean Temperature Gradient", *Int. J. Heat Mass Transfer*, Vol. 41, pp. 3627-3634.

Moser, R.D. and Moin, P., 1987, "The Effects of Curvature in Wall-Bounded Turbulent Flows", *J. Fluid Mech.*, Vol. 175, pp. 479-510 (1987).

Ohta, T. and Kajishima, T., 2004, "DNS of Turbulent Channel Flow Subjected to the Acceleration", *Transactions of the Japan Society of Mechanical Engineers, Series B*, Vol. 70, No. 696, pp. 1903-1910.